Eur. Phys. J. C (2022) 82:478
https://doi.org/10.1140/epjc/s10052-022-10416-8

THE EUROPEAN PHYSICAL JOURNAL C

Regular Article - Theoretical Physics

Alternating current conductivity and superconducting properties of a holographic effective model with broken translations

Yan Liu[1], **Xi-Jing Wang**[2], **Jian-Pin Wu**[2,a], **Xin Zhang**[1,3,4,b]

[1] Department of Physics, College of Sciences, Northeastern University, Shenyang 110819, China
[2] Center for Gravitation and Cosmology, College of Physical Science and Technology, Yangzhou University, Yangzhou 225009, China
[3] Frontiers Science Center for Industrial Intelligence and Systems Optimization, Northeastern University, Shenyang 110819, China
[4] Key Laboratory of Data Analytics and Optimization for Smart Industry (Northeastern University), Ministry of Education, Shenyang 110819, China

Received: 26 January 2022 / Accepted: 9 May 2022 / Published online: 24 May 2022

Abstract We construct a holographic effective superconducting theory by considering a special gauge-axion coupling. In the normal state, we observe that a peak emerges in the mid-IR in the AC conductivity for certain strength of broken translations and the gauge-axion coupling. It is attributed to the emergence of pseudo-Goldstone mode due to the competition of spontaneous symmetry breaking (SSB) and the explicit symmetry breaking (ESB). However, when the ESB dominates over the SSB, the peak disappears. In the superconducting phase, this gauge-axion coupling also plays a key role leading to a more evident gap at the low frequency conductivity. In addition, we also study the combined effects of the strength of broken translations and various couplings among the gauge field, axion fields and the complex scalar field.

Contents

[a] e-mail: jianpinwu@yzu.edu.cn (corresponding author)
[b] e-mail: zhangxin@mail.neu.edu.cn

1 Introduction

The Bardeen–Cooper–Schrieffer (BCS) theory [1,2] is a successful microscopic theory to describe the superconductivity discovered in 1911 [3], in which the condensate is understood from Cooper pairs of electrons bound together by phonons. The electron-phonon interactions are much weaker, however in high temperature superconductors and the mechanism behind high temperature superconductivity is thus believed beyond the framework considered in BCS theory. Many scientists have been trying to reveal the basic principle behind them. But until now it still has no satisfied microscopic description for the high temperature superconductivity.

Alternatively, AdS/CFT correspondence [4–7], or more generally referring to holography, provides an effective description for the high temperature superconductors and also opens up a new window for studying the mechanism of the high temperature superconductivity. The main idea of holography is that a strongly coupled quantum field theory can be mapped to a higher-dimensional bulk gravity system. Based on this idea, a pioneering holographic superconductor model is proposed by Hartnoll, Herzog, and Horowitz (HHH) [8,9]. This model exists two states: the superconducting state with a non-vanishing charge condensate and the normal state of a perfect conductor. It means that there exists an infinite electric direct current (DC) conductivity even in the normal state due to the translational invariance of the system. To construct a more realistic superconductor model, it is important to break the translational invariance in the holographic framework such that we have a momentum dissipation system.

There are several ways to break the translational invariance in the bulk gravity. The most brutal way is to introduce a spatially-dependent source in the dual boundary theory. It has

been implemented by a spatially-periodic real scalar source or chemical potential [10–14]. They are usually referred to as the scalar lattice and the ionic lattice, respectively. In this method, such spatially-dependent sources typically lead to the inhomogeneity of the dynamic fields in the bulk, which generate a set of complicated coupled partial differential equations (PDEs). Though conceptually clear, the application of this framework is limited by numerical technology. This is because the accuracy of solving PDE numerically depends heavily on the temperature of the background. Thus, it is extremely difficult to explore the lattice effects at the extremely low temperature [15].

To bypass the technical complexity of solving the PDEs but capture the important aspect of the momentum dissipation, people develop a much simpler but elegant mechanism to break the translation symmetry but retain the homogeneity of the background geometry, for which we only need solve the ordinary differential equations (ODEs). So far, several models have been proposed to implement this mechanism, including holographic Q-lattices [16–19], helical lattices [20] and axions model [21–33]. Holographic Q-lattice model implements the breaking of the translational symmetry by the global phase of the complex scalar field. Holographic helical lattice model possesses the non-Abelian Bianchi VII_0 symmetry, which results in the translational symmetry breaking but holds homogeneous background geometry. The simplest model is the so-called holographic axions model [21], which breaks the translational symmetry by a pair of linearly spatial-dependent scalar fields. Then, guiding in the spirit of effective holographic low energy theories, it is natural and interesting to explore the effect of higher-derivative terms of axion fields [34–37]. The higher-derivative effect turns out to have a heavy impact on the lower bound of charge diffusion [34] but have no effect on its upper bound [37]. Such higher-derivative term has no impact on the bound of energy diffusion [34]. It was also found that the lower bound of DC conductivity of the usual axions model [21] can be violated in the holographic effective theory with higher-derivative terms [35,38], such that we have vanishing DC conductivity at zero temperature, which provides a framework to model a more realistic insulating state. In this holographic effective framework, the spontaneous symmetry breaking (SSB), which is associated with the gapless excitations called Goldstone modes in the low energy description, and the so-called pseudo-SSB associated with the pseudo-Goldstone mode, where the SSB dominates over the explicit symmetry breaking (ESB), can be implemented [36,39–44]. We would like to point out that the holographic massive gravity studied in [45] also belongs to the framework of holographic effective axionic model. For the detailed discussions, please refer to [46]. In addition, we can also achieve the momentum dissipation in the dual boundary field theory by introducing a higher-derivative interaction term between the $U(1)$ gauge field and the scalar field, which spontaneously generates a spatially dependent profile of the scalar field [47,48].

The holographic superconductor models with broken translations have also been constructed and studied [49–58]. In Ref. [49], a pioneering work of holographic lattice superconductor model implemented by a periodic potential was set up. They reproduced some qualitative features of some cuprates, including the superconducting energy gap and the power law fall-off at the intermediate frequency. The holographic Q-lattice superconductor was also built in [50,57]. Their result demonstrates that the condensate of the scalar field would be suppressed by the lattice effects and thus leads to a lower critical temperature. In particular, they found that if the normal state is a deep insulating phase, the condensation never happens for small charge of the scalar field. Moreover in holographic superconductor with axion fields [51], the authors found the existence of a new type of superconductor induced by the strength of momentum relaxation even at chemical potential being zero. It means that there exists a new "pairing" mechanism of particles and antiparticles interacting with the strength of momentum relaxation. In Ref. [58], a more phenomenologically relevant holographic superconducting model of momentum dissipation was constructed based on Gubser-Rocha model whose ground state entropy vanishes [59]. It was also shown that some universal properties of high T_c superconductors, including linear-T resistivity near T_c and Homes' law, are observed [58]. In addition, a superconducting dome-shaped region is implemented on the temperature-doping phase diagram in holographic axion superconductor proposed in [56].

In this paper, we shall construct an effective holographic superconductor with broken translations, for which the higher derivative terms of axion fields are introduced. We intend to study the alternating current (AC) conductivity over the normal state and the superconducting properties of this effective holographic superconductor. The plan of this work is as follows: In Sect. 2, we construct the effective holographic model with broken translations. In Sect. 3, we study the conductivity in the normal state. The superconducting properties are explored in Sect. 4. In Sect. 5, we conclude.

2 Holographic framework

In this section, we construct an effective holographic superconductor model with broken translations. It includes the following key ingredients: the metric $g_{\mu\nu}$, $U(1)$ gauge field A_μ, the complex scalar field ψ and two axionic fields X^I $(I = x, y)$ with x, y being spatial coordinates. The superconducting phase is supported by the complex scalar field ψ, which can be defined by $\psi = \chi e^{i\theta}$ with χ being the real scalar field and θ being the Stückelberg field. A pair of spatial

linear dependent axionic fields result in the breaking of the translation symmetry.

Including all the ingredients, we write down the total action of the model as

$$S=\int d^4x\sqrt{-g}\Big(R+6+\mathcal{L}_M+\mathcal{L}_\chi+\mathcal{L}_X\Big), \tag{1}$$

$$\mathcal{L}_M=-\frac{Z(\chi)}{4}F^2, \tag{2}$$

$$\mathcal{L}_\chi=-\frac{1}{2}(\partial_\mu\chi)^2-H(\chi)(\partial_\mu\theta-qA_\mu)^2-V_{\rm int}(\chi), \tag{3}$$

$$\mathcal{L}_X=-\frac{J(\chi)}{4}{\rm Tr}[XF^2]-V(X). \tag{4}$$

$F_{\mu\nu}=\nabla_\mu A_\nu-\nabla_\nu A_\mu$ is the field strength of gauge field A_μ. The coupling function of Maxwell field strength takes the form as

$$Z(\chi)=1+\frac{a\chi^2}{2}. \tag{5}$$

We define $X\equiv{\rm Tr}[X^\mu{}_\nu]$ with

$$X^\mu{}_\nu=\frac{1}{2}\partial^\mu X^I\partial_\nu X^I, \tag{6}$$

where $I=x,y$. The potential $V(X)$ in the Lagrangian density $\mathcal{L}_X$ is

$$V(X)=X\,, \tag{7}$$

which is just the simplest axion term proposed in Ref. [21]. As in Refs. [34–36], we introduce a higher derivative term of axion fields coupled with the gauge field as[1]

$${\rm Tr}[XF^2]\equiv X^\mu{}_\nu F^\nu{}_\rho F^\rho{}_\mu. \tag{8}$$

The coupling coefficient $J(\chi)$ takes the form

$$J(\chi)=\alpha_1+\frac{\alpha_2\chi^2}{2}. \tag{9}$$

In the normal state, the setup is closely similar to that in [36]. The term $V(X)=X$ and the gauge-axion term play the role of ESB and SSB, respectively. In our setup, α_1 controls the SSB, while α controls both the ESB and SSB. However, in the setup of [36], the ESB and SSB can be independently controlled. We shall further discuss the roles of the term $V(X)=X$ and the gauge-axion term in next section.

$\mathcal{L}_\chi$ is the Lagrangian density supporting the superconducting phase transition. The coupling function $H(\chi)$ and the potential $V_{\rm int}(\chi)$ are given by

$$H(\chi)=\frac{n\chi^2}{2},\quad V_{int}(\chi)=\frac{M^2\chi^2}{2}, \tag{10}$$

where M is the mass of the scalar field ψ. Without loss of generality, we choose the gauge $\theta=0$ in what follows.

[1] There is another formula of gauge-axion couplings, for instance, $K\,{\rm Tr}[X]F^2$ [34,35,60,61].

From the action above, we derive the covariant form of the equations of motion:

$$\nabla_\mu\Big[ZF^{\mu\nu}-\frac{J}{2}\Big((XF)^{\mu\nu}-(XF)^{\nu\mu}\Big)\Big]-2Hq^2A^\mu=0, \tag{11}$$

$$\nabla_\mu\nabla^\mu\chi-\partial_\chi Hq^2A^2-\frac{\partial_\chi Z}{4}F^2-\frac{\partial_\chi J}{4}{\rm Tr}[XF^2]-\partial_\chi V_{int}=0, \tag{12}$$

$$\nabla_\mu\Big[\nabla^\mu\phi^I+\frac{J}{4}(F^2)^\mu{}_\nu\nabla^\nu\phi^I\Big]=0, \tag{13}$$

and

$$R_{\mu\nu}-\frac{1}{2}g_{\mu\nu}R-3g_{\mu\nu}-\frac{1}{2}\nabla_\mu\phi\nabla_\nu\phi-\frac{1}{2}\nabla_\mu\chi\nabla_\nu\chi-Hq^2A_\mu A_\nu-\frac{Z}{2}F_{\mu\rho}F_\nu{}^\rho-\frac{J}{4}\Big(\frac{1}{2}\nabla_{(\mu|}\phi^I\nabla_\sigma\phi^I(F^2)^\sigma{}_{|\nu)}+F_{(\mu|\sigma}(FX)^\sigma{}_{|\nu)}+F_{(\mu|\sigma}(XF)^\sigma{}_{|\nu)}\Big)-\frac{1}{2}g_{\mu\nu}(\mathcal{L}_M+\mathcal{L}_\chi+\mathcal{L}_X)=0, \tag{14}$$

where the symmetry brackets above mean $A_{(\mu\nu)}=(A_{\mu\nu}+A_{\nu\mu})/2$.

To solve the above equations, we take the following ansatz

$$\begin{aligned}ds^2&=\frac{1}{u^2}\Big[-(1-u)p(u)U_1dt^2+\frac{du^2}{(1-u)p(u)U_1}\\&\quad+U_2dx^2+U_2dy^2\Big],\\A_t&=\mu(1-u)b(u),\quad\chi=u^{3-\Delta}\phi,\\X^x&=\alpha x,\quad X^y=\alpha y,\end{aligned} \tag{15}$$

with $p(u)=1+u+u^2-\mu^2u^3/4$ and $\Delta=3/2\pm(9/4+M^2)^{1/2}$. $u=1$ is the black hole horizon while the AdS boundary locates at $u=0$. α is a constant denoting the strength of broken translations. U_1 and U_2 are just the function of the radial coordinate u. We impose the boundary condition $U_1(1)=1$ at the horizon so that we have the temperature of the dual system as

$$T=\frac{3}{4\pi}-\frac{\mu^2}{16\pi}. \tag{16}$$

Through this paper we take $M^2=-2$ such that $\Delta=2$. Then for given coupling parameters a, α_1, α_2 and n, this holographic system is depicted by the dimensionless Hawking temperature T/μ and the strength of broken translations α/μ. For convenience, we abbreviate the two dimensionless quantities $\{T/\mu,\alpha/\mu\}$ to $\{T,\alpha\}$ in the following.

3 Conductivity in normal phase

Obviously, in the case of $\chi=0$, the action describes the non-superconducting phase. In the case of $\chi=0$, the black hole

solution can be analytically worked out. It is found that the gauge-axion coupling has no effect on the background solution and this exact background solution is just the Reissner–Nordström-AdS (RN-AdS) black hole solution with axions [21]. Here for numerical convenience, we still take the ansatz (15) to solve the background of the normal state.

Before proceeding, we would like to further explain the roles of the two terms in the Lagrangian density $\mathcal{L}_X$ (Eq. (4)). To this end, we assume that the axionic fields X^I depend on the full coordinates x^μ. If we only consider the usual axion term, i.e., the second term of $\mathcal{L}_X$, the asymptotic behavior of X^I near the AdS boundary is [36,44]

$$X^I = X_I^{(0)}(t, x^i) + X_I^{(3)}(t, x^i)u^3 + \cdots . \tag{17}$$

Following the standard quantization, $X_I^{(0)}(t, x^i)$ is the source of the dual operator and $X_I^{(3)}(t, x^i)$ is interpreted as the expectation value. The special profile of axionic fields $X^I = \alpha x^i$ means the source also has the form $X_I^{(0)}(t, x^i) = \alpha x^i$ in the dual field theory. It indicates that the breaking of the symmetry is explicit.

If only the first term of $\mathcal{L}_X$ survives, the axionic fields near the AdS boundary behave like [36,44]

$$X^I = X_I^{(-1)}(t, x^i)u^{-1} + X_I^{(0)}(t, x^i) + \cdots . \tag{18}$$

Now, the subleading term is the second one in the above expansion and should be interpreted as the expectation value $\langle \mathcal{O}^I \rangle \sim \alpha \delta_i^I x^i$ with a vanishing source [36]. It means that a SSB appears, which is associated with the gapless excitations called Goldstone modes in the low energy description.

If the first term dominates over the second term in the Lagrangian density $\mathcal{L}_X$, the system shall be weak explicit symmetry breaking, which leads to a slightly gapped excitation and means the emergence of the pseudo-Goldstone mode [44]. It is obvious that in our setup, α_1 controls the SSB, while α controls both the ESB and SSB.

Next, we shall study the DC and AC conductivities over the normal state, respectively.

3.1 DC conductivity

Though the gauge-axion coupling has no effect on the background solution, it enters into the perturbative equations leading to strong impact on the transports, which has been seen in the properties of DC transports [34–36]. For completeness, we shall give a brief review on DC conductivity over the normal state in this subsection.

Based on "membrane paradigm" [62,63] (see also [64–66]), we can analytically work out DC conductivity determined by the background data at the horizon. According to the pivotal point of this method, we construct a radially conserved current $\mathcal{J}$ connecting the horizon and the boundary. At this stage, we can calculate DC conductivity as

$$\sigma_{DC} = -\frac{(\alpha^2\mu^2\alpha_1 - 4U_2(1))(\alpha^2\mu^2 + \mu^2 b^2(1)U_2(1))}{\alpha^2\mu^2(4 + \alpha_1\mu^2 b^2(1))U_2(1)}. \tag{19}$$

Obviously, different from the simplest axionic model [21], DC conductivity from the higher-derivative corrections depends on the temperature T and also the broken translations strength α. Notice that the requirement of the positive definiteness of the conductivity imposes a constraint on the coupling parameter α_1 as $0 \leq \alpha_1 \leq 2/3$ [35].

We plot DC conductivity with the coupling parameter α_1 turned on in the top left in Fig. 1. The plot is exhibited to demonstrate DC conductivity as the function of α at zero temperature. It is easy to find that at zero temperature, when the coupling parameter α_1 increases, DC conductivity decreases with α increasing. In particular, for $\alpha_1 = 2/3$, the DC conductivity tends to zero with α increasing, which violates the DC conductivity bound in the simplest holographic axion model [21]. Notice that in the limit of $\alpha \to 0$, due to the restoration of the violation of the translational symmetry, the DC conductivity tends to α_1-independent infinity.

In holographic system, the temperature behavior of DC conductivity can well describe some characteristics of the system. In particular, in many holographic references [16–20,38,66–74], people often adopt the so-called operational definition to identify the metallic phase and insulating phase, i.e.,

- Metallic phase: $\partial_T \sigma_{DC} < 0$.
- Insulating phase: $\partial_T \sigma_{DC} > 0$.
- Critical point (line): $\partial_T \sigma_{DC} = 0$.

Here we also study the temperature behaviors of DC conductivity, which are shown in the rest plots in Fig. 1. When the higher-derivative term is absent, i.e., $\alpha_1 = 0$, σ_{DC} is independent of the temperature. Once the coupling parameter α_1 is turned on, DC conductivity decreases with T decreasing. In terms of the operational definition of phase of the holographic system described above, this holographic system exhibits the insulating behavior. But we note that unless α_1 takes the bounded value $\alpha_1 = 2/3$ and α tends to infinity, DC conductivity cannot vanish in the limit of zero temperature. For the fixed α, σ_{DC} decreases with α_1 increasing.

3.2 AC conductivity

In this subsection, we numerically calculate AC conductivity in the normal state. Since our system is homogeneous and isotropy, it is enough to turn on the following consistent linear

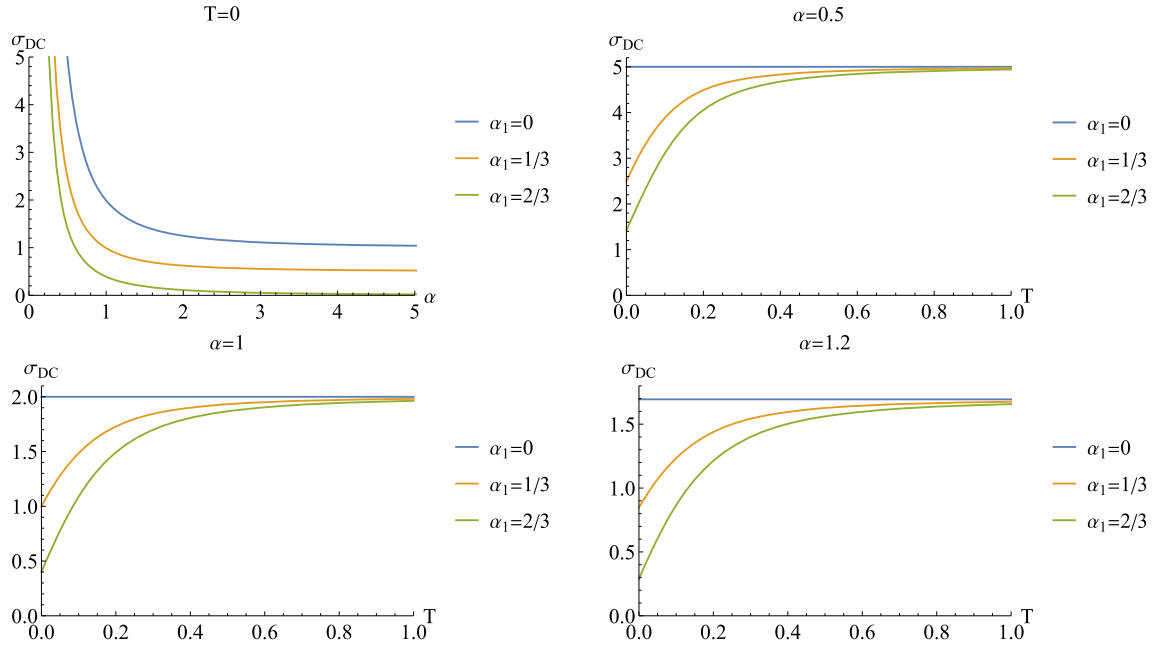

Fig. 1 The DC conductivity with the α_1 coupling turned on by setting $T = 0$ while α vary and by setting $\alpha = \{0.5, 1, 1.2\}$ while T vary. Here we have abbreviated the two dimensionless quantities $\{T/\mu, \alpha/\mu\}$ to $\{T, \alpha\}$

perturbation

$$\delta A_x(t,u,x^i) = \int_{-\infty}^{+\infty} \frac{d\omega}{(2\pi)^3} e^{-i\omega t}\delta b_x(u),$$
$$\delta g_{tx}(t,u,x^i) = \int_{-\infty}^{+\infty} \frac{d\omega}{(2\pi)^3} e^{-i\omega t}u^{-2}h_{tx}(u),$$
$$\delta X^x(t,u,x^i) = \int_{-\infty}^{+\infty} \frac{d\omega}{(2\pi)^3} e^{-i\omega t}\delta\phi^x(u). \quad (20)$$

Thus we shall have three ordinary differential equations for $h_{tx}, \delta b_x, \delta\phi^x$. It turns out that near the UV boundary ($u \to 0$), the asymptotic behavior of the Maxwell field falls in the following form

$$\delta b_x = b^{(0)} + b^{(1)}u + \cdots . \quad (21)$$

According to holographic dictionary, we read off the conductivity as

$$\sigma(\omega) = -\frac{ib^{(1)}}{\omega b^{(0)}}. \quad (22)$$

Then, we shall impose the ingoing boundary condition at the horizon to solve the perturbative system and read off the conductivity as the function of the frequency in terms of Eq. (22).

Figure 2 exhibits the real and imaginary parts of AC conductivity in the normal state at $T = 0.015$. At the high frequency regime, $\omega \gg \mu$, the conductivity tends towards a constant determined by ultraviolet (UV) CFT fixed point. The interesting physics lies at the low frequency region.

Before proceeding, we present some comments on the AC conductivity behavior at low frequency without gauge-axion coupling ($\alpha_1 = 0$) [21], where the translation symmetry is explicitly broken. For this case, we observe that AC conductivity in real part displays a standard Drude peak at low frequency when the momentum dissipation is weak, i.e., α is small. It implies that the weak momentum dissipation drives the current into a coherent state. Theoretically, it is because the total momentum of the system is approximately conserved, for which we can implement a perturbative expansion in the small momentum relaxation rate within the memory matrix formalism [75–78]. With the strength of the momentum dissipation increasing, the Drude peak gradually reduces and we observe a transition from coherent phase to incoherent phase (see the blue curves in Fig. 2, also see Refs. [23,79]). In fact, because we must include the contribution at subleading order in the relaxation rate when the momentum dissipation is strong, the behavior of AC conductivity at low frequency should be depicted by a modified holographic formula, first derived in [80] and generalized to a more general holographic theory [81], instead of the standard Drude formula or even the modified hydrodynamic results.

However, when the gauge-axion coupling term $\alpha_1 Tr[XF^2]$ in the Lagrangian density Eq. (4), which controls the SSB, is introduced. AC conductivity exhibits some interesting behaviors. Recalling that in this model the strength of broken translations α controls both the ESB and SSB. From the first and second rows in Fig. 2, we see that a peak emerges

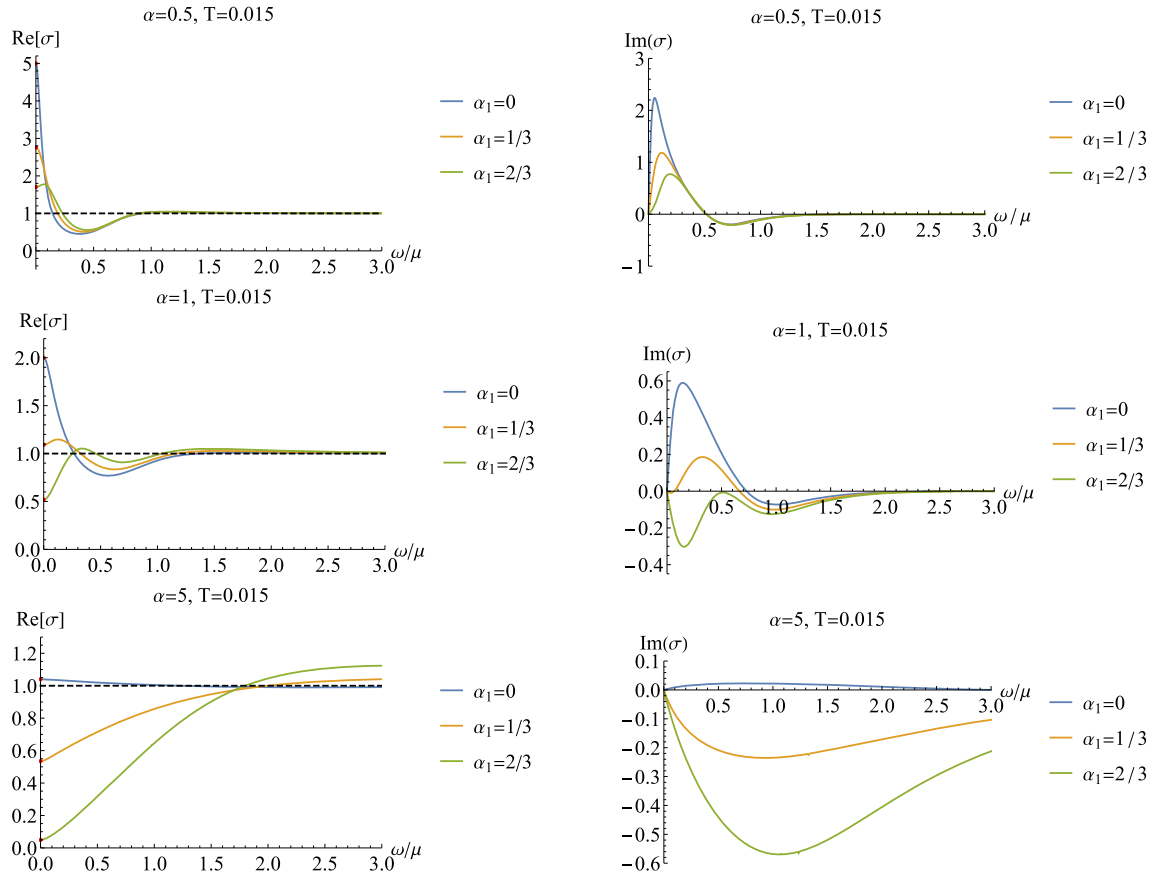

Fig. 2 AC conductivity in the normal state at $T = 0.015$ with different α and α_1. The red dots correspond to DC conductivity obtained from formula (19). Here we have abbreviated the two dimensionless quantities $\{T/\mu, \alpha/\mu\}$ to $\{T, \alpha\}$

in the mid-IR in the AC conductivity for some α and α_1. The peak moves to higher energy with α_1 or α increasing (the first and second rows in Fig. 2). As discussed at the beginning of this section (also refer to Refs. [36,44]), this peak attributes to the emergence of the pseudo-Goldstone mode, which is the result of the competition of SSB and ESB. Notice that in the setup of Ref. [36], they can separately control the strength of SSB and ESB to make the ESB is weak compared with the SSB such that the peak in min-IR is more pronounced. However, when the ESB dominates over the SSB (α_1 small or α too large), the peak in min-IR disappears (see the third row in Fig. 2).

4 Superconducting phase

In this section, we turn to study the superconducting properties of this holographic effective theory with gauge-axion coupling. Some works have studied the superconducting properties of holographic axion model [51,52,56,82,83]. Here, we shall mainly focus on the effect of gauge-axion coupling.

4.1 Condensation

Under the ansatz (15), we numerically solve the equations of motion (11)–(14) to explore the properties of the condensation. Again, it is easy to find that the gauge-axion coupling term $J\mathrm{Tr}[XF^2]$ has no any effect on the background solution even in the superconducting phase. Only three parameters: the strength of broken translations α, the gauge coupling parameters a and n, exert their influence on the condensation. Notice that from the Lagrangian density $\mathcal{L}_\chi$, i.e., Eq. (3), we see that the relevant quantity is the product of q and n. At the same time, since the increase of charge makes the condensation easier, which had been widely studied in previous references for example [49,50], we shall set $q = 2$ and $n = 1$ through this paper without loss of generality.

In the unit of the critical temperature we plot the condensation $< O_2 >$ as a function of the temperature by fixing the gauge coupling parameter a or by fixing the strength of broken translations α, respectively. When we fix the gauge coupling parameter a, the stronger the strength of broken translations, the expectation value of the condensation becomes much larger and thus the critical temperature becomes lower (Fig. 3), which had also been observed in many works for

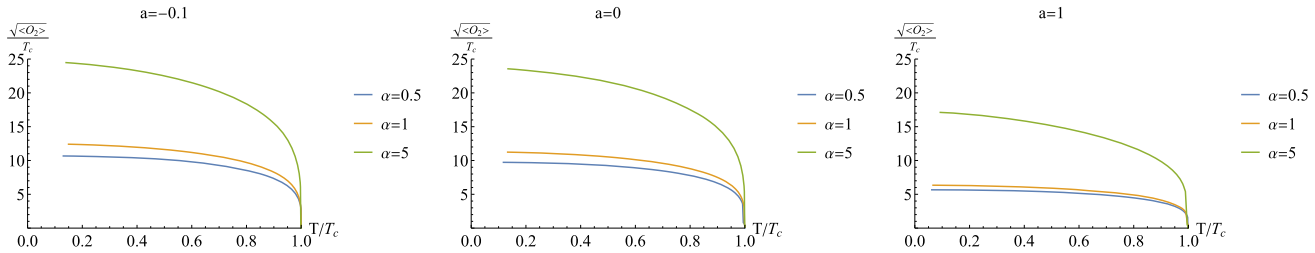

Fig. 3 The condensation $< O_2 >$ as a function of temperature for given a (from left to right $a = -0.1$, $a = 0$ and $a = 1$) and various values of α. We have set $q = 2$ and $n = 1$. Here we have abbreviated the two dimensionless quantities $\{T/\mu, \alpha/\mu\}$ to $\{T, \alpha\}$

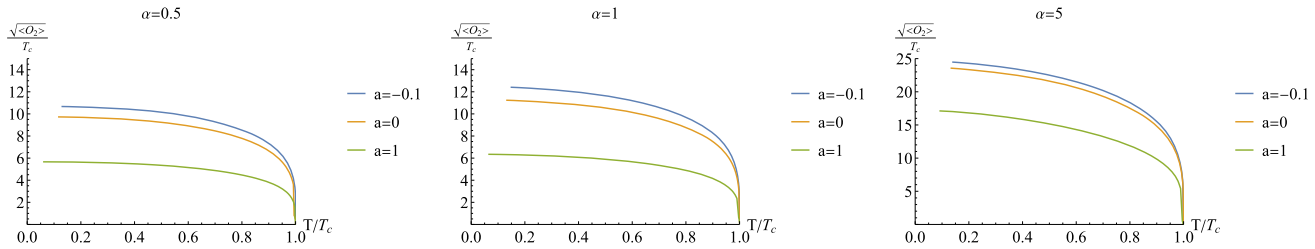

Fig. 4 The condensation $< O_2 >$ as a function of temperature for given α (from left to right $\alpha = 0.5$, $\alpha = 1$ and $\alpha = 5$) and various values of a. We have set $q = 2$ and $n = 1$. Here we have abbreviated the two dimensionless quantities $\{T/\mu, \alpha/\mu\}$ to $\{T, \alpha\}$

example [50,51,53]. Therefore, we conclude that the condensation becomes harder with the strength of broken translations increasing even in presence of the gauge coupling. We expect that the condensation is violated as the broken translations becomes stronger beyond some critical values.

And then, we fix the strength of broken translations α and vary the gauge coupling parameter a to see the effects of gauge coupling on the condensation. From Fig. 4, we see that with a increasing, the expectation value of the condensate becomes much smaller. It indicates that the condensation becomes easier and the critical temperature becomes higher.

4.2 Superconducting conductivity

To calculate AC conductivity in the superconducting phase, we can follow the same procedure in the normal state outlined in Sect. 3.2. Different from the condensation, there are four theory parameters $(\alpha, a, \alpha_1, \alpha_2)$ affecting the superconducting conductivity. In what follows, we shall explore the effects of these coupling parameters on the conductivity step by step.

We first study the effects of the momentum dissipation on AC conductivity. To this end, we turn off the other coupling parameters. In Fig. 5, we plot the real and imaginary parts of AC conductivity as a function of frequency for various α. We also show the evolution of the conductivity with the temperature from normal phase to superconducting phase. We observe that once the system enters into the superconducting phase, the imaginary part of the conductivity climbs up rapidly and tends to infinity in the limit of $\omega = 0$. According to the Kramers-Kronig (KK) relation, a pole emerges in $Im[\sigma]$ implying a corresponding delta function in $Re[\sigma]$, which is one of the hallmarks of genuine superconductor. In order to exhibit such sudden change more distinctly, we plot the conductivity in low frequency region with the temperature dropping through the critical point in Fig. 6. Unlike the abrupt changing behavior of the imaginary part, the real part of the conductivity only changes slightly near the critical temperature. The real part of optical conductivity at low frequency goes down with the temperature decreasing and finally vanishes at extremal low temperature. In addition, we also work out the normal fluid density n_n defined by

$$n_n = \lim_{\omega \to 0} Re[\sigma(\omega)]. \tag{23}$$

which depicts the contribution from the normal, non-superconducting component on the DC conductivity in the superconducting phase. The results are showed in Table 1. It is found that the values of n_n are still finite when the system just enters the superconducting phase, while n_n goes down with the temperature decreasing and vanishes at extremal low temperature. Therefore, our holographic model also resembles a two-fluid model as the standard holographic superconductor model [8,9,84], the holographic Q-lattice superconductor [50], and the holographic superconductor from higher derivative theory [85,86].

Furthermore, we study the combined effect of the strength of broken translations α and the gauge coupling parameter a in the superconducting state. Here we have fixed the remaining parameters (α_1 and α_2) to be zero. In Fig. 7, we show both real and imaginary parts of conductivity with different a and α. At low temperature ($T/T_c \approx 0.2$), the real part of the conductivity tends to zero in the limit of $\omega \to 0$ (see

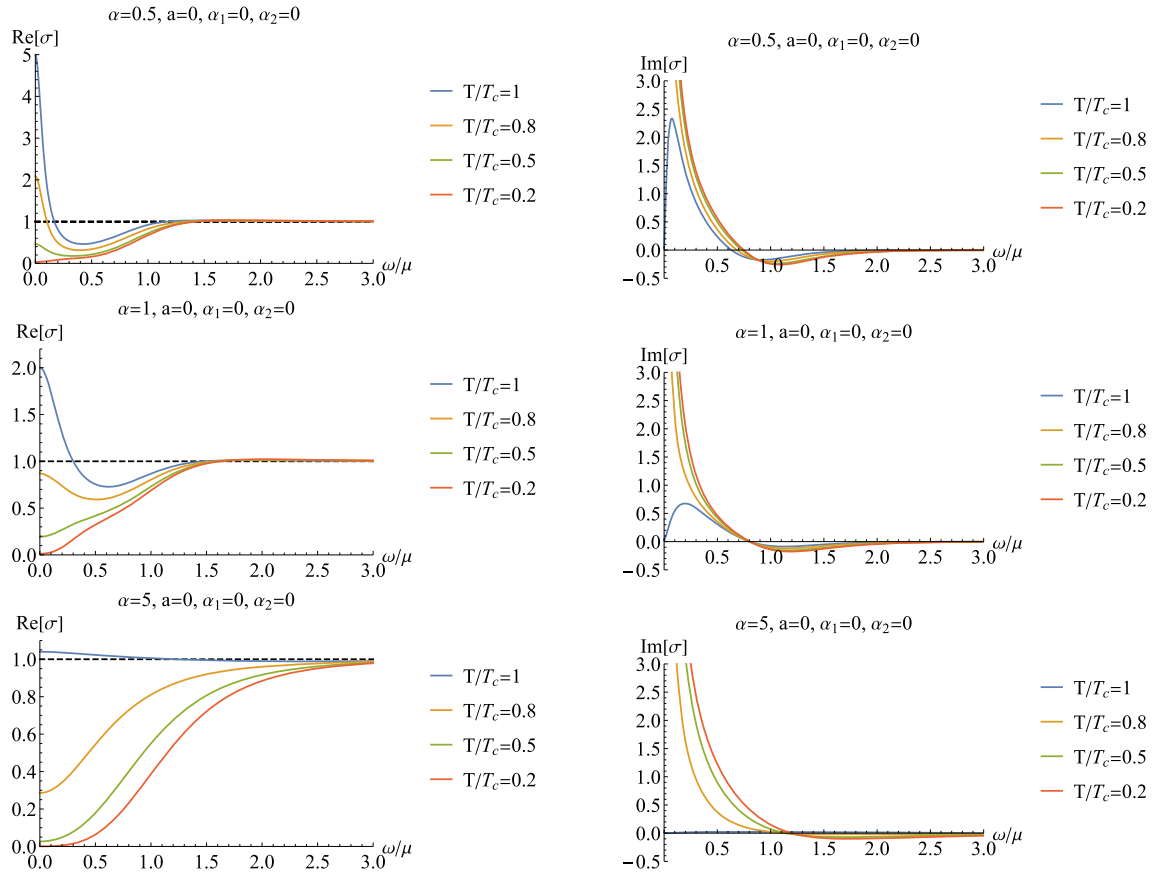

Fig. 5 The conductivities σ as a function of the frequency for different α fixing $a = 0$, $\alpha_1 = 0$, and $\alpha_2 = 0$. The left panels are for the real part and the right panels are for the imaginary one. Here we have abbreviated the two dimensionless quantities $\{T/\mu, \alpha/\mu\}$ to $\{T, \alpha\}$

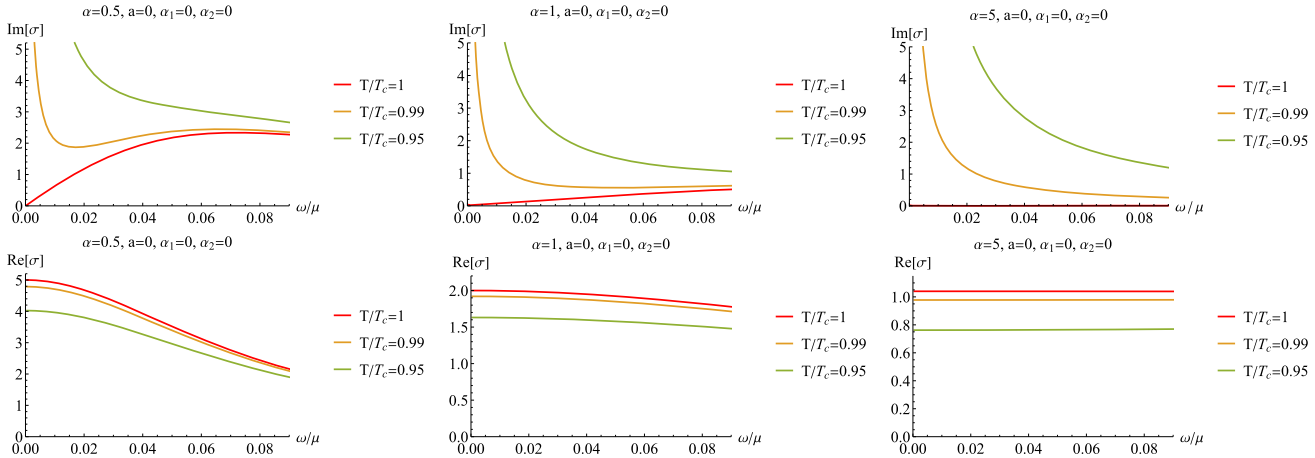

Fig. 6 The critical behavior of the conductivity near the critical temperature in the low frequency region for the different α. We have turned off other coupling parameters. Here we have abbreviated the two dimensionless quantities $\{T/\mu, \alpha/\mu\}$ to $\{T, \alpha\}$

Table 1 The normal fluid density n_n in the superconducting phase for the different temperature with different α. Here we turned off other coupling parameters and the dimensionless quantity $\{\alpha/\mu\}$ is abbreviated as $\{\alpha\}$

n_n	$\frac{T}{T_c} = 1$	$\frac{T}{T_c} = 0.95$	$\frac{T}{T_c} = 0.90$	$\frac{T}{T_c} = 0.85$	$\frac{T}{T_c} = 0.80$	$\frac{T}{T_c} = 0.50$	$\frac{T}{T_c} = 0.20$
$\alpha = 0.5$	5	4.0230	3.2377	2.6031	2.0873	0.4624	0.0307
$\alpha = 1$	1.9999	1.6311	1.3280	1.0778	0.8706	0.1929	0.0118
$\alpha = 5$	1.0400	0.7622	0.5549	0.4004	0.2858	0.0266	0.0006

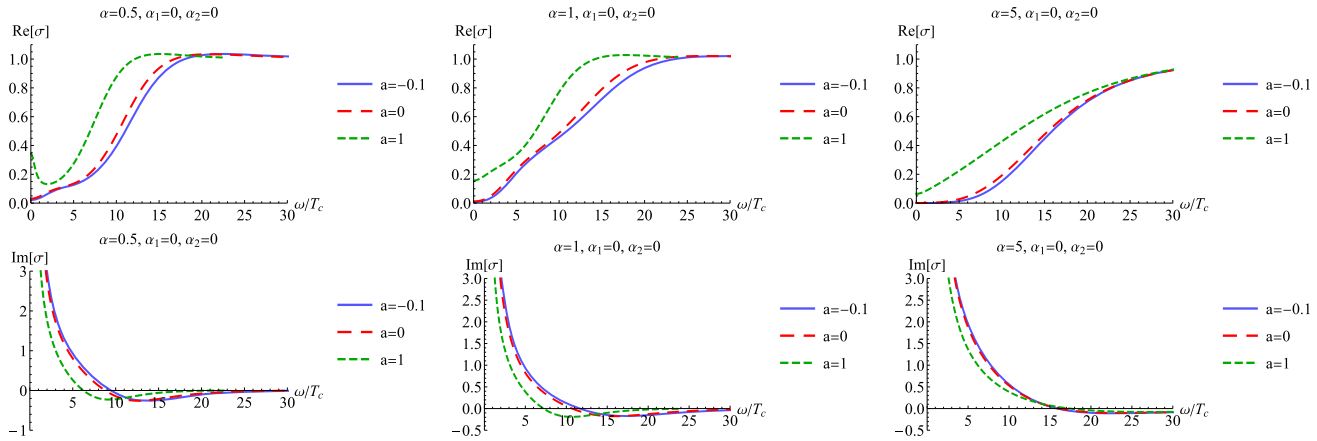

Fig. 7 The behavior of conductivity with varying a for different α in the superconducting state. Here we fix the temperature $T/T_c \approx 0.2$. Here we have abbreviated the two dimensionless quantities $\{T/\mu, \alpha/\mu\}$ to $\{T, \alpha\}$

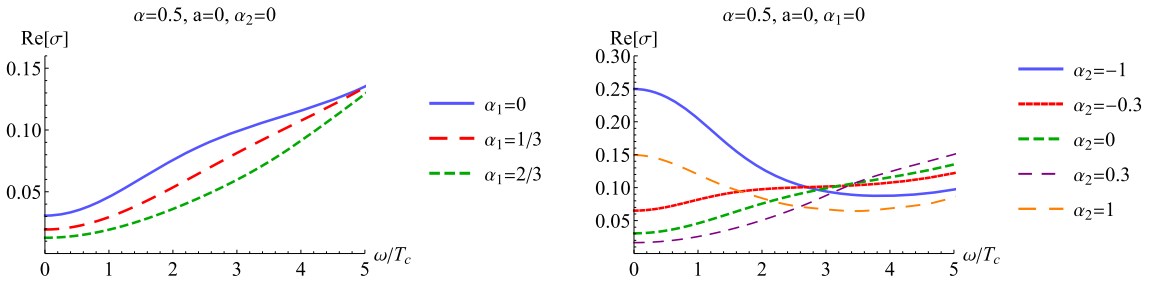

Fig. 8 The real part of conductivity as the function of the frequency at $T/T_c \approx 0.2$. Left plot: different α_1 for $\alpha = 0.5$, $a = 0$ and $\alpha_2 = 0$. Right plot: different α_2 for $\alpha = 0.5$, $a = 0$ and $\alpha_1 = 0$. Here we have abbreviated the two dimensionless quantities $\{T/\mu, \alpha/\mu\}$ to $\{T, \alpha\}$

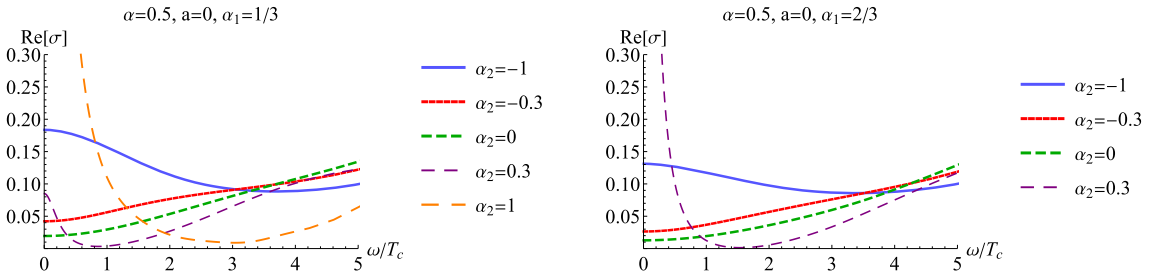

Fig. 9 The real part of conductivity as the function of the frequency with various α_2 for fixed $\alpha = 0.5$ and $a = 0$ at $T/T_c \approx 0.2$. Left plot is for $\alpha_1 = 1/3$ and right plot for $\alpha_1 = 2/3$. Here we have abbreviated the two dimensionless quantities $\{T/\mu, \alpha/\mu\}$ to $\{T, \alpha\}$

the dashed red lines in Fig. 7 and also see Fig. 5). It implies that at this temperature, most of the normal components of the electron fluid have formed the superfluid component. For negative a ($a = -0.1$), the case is similar to that of $a = 0$. However, for positive a ($a = 1$), the DC conductivity starts to rise up. It means that we need further cool the system to drive the normal component of the electron fluid forming the superfluid component.

We also explore the impact of gauge-axion coupling parameters (α_1 and α_2) on the optical conductivity in the superconducting state. The results are exhibited in Figs. 8 and 9. In order to avoid the effect of gauge parameter a on the conductivity, here we fix $a = 0$. In addition, we also set $\alpha = 0.5$ without loss of generality. We summarize the main effects of the gauge-axion coupling as what follows:

- Increasing the gauge-axion coupling α_1, it is easier to drive the normal component of the electron fluid forming the superfluid component and the superconducting energy gap becomes evident (left plot in Fig. 8). We also observe that the peak in the mid-IR in the normal state is smoothed out when the system enters into the superconducting phase.
- To see the effect from the coupling α_2, which is a coupling among gauge field, axion fields and complex scalar field being responsible for condensation, we turn off α_1. The

low frequency behaviors of conductivity are exhibited in the right plot in Fig. 8. For negative α_2, DC conductivity rises up with the absolute value of α_2 increasing and then the conductivity forms a small peak at low frequency for large absolute value of α_2. For positive α_2, we see that with α_2 increasing, DC conductivity goes down at first and then rises up exhibiting a non-linear change. When α_2 rises up to a large value, the conductivity also sprouts up a small peak at low frequency. Based on these observations, it is obvious that the role α_2 playing is completely different from that of α_1. We attribute this difference to the effect of condensation field χ. Furthermore, we would like to point out that the mechanism of this small peak emerging at low frequency deserving further pursuit.

- We further study the combined effects of the coupling α_1 and α_2, and also the competition between them. Fig. 9 shows the real part of conductivity with various α_2 for fixed $\alpha_1 = 1/3$ (left plot) and $\alpha_1 = 2/3$ (right plot). It is clear that for negative α_2, DC conductivity is suppressed with the increase of α_1.
- However, for positive α_2, the effect of the coupling term α_2 dominates over that of the coupling term α_1. From Fig. 9, we see that once the coupling terms α_1 and α_2 are both turned on, a peak emerges at low frequency. Recalling that for $\alpha_1 = 0$, a gap is evident at low frequency even for $\alpha_2 = 0.3$. With α_1 increasing, the peak at low frequency becomes more evident.

5 Conclusion

In this paper, we construct a holographic effective superconducting theory including some coupling terms among the gauge field, axion fields and complex scalar field. In the normal state, this holographic effective superconducting theory reduces to the so-called $\mathcal{J}$ model studied in Refs. [35,36]. In the normal state, though the gauge coupling term $\alpha_1 \mathrm{Tr}[XF^2]$ has no effect on the background solution, it enters into the perturbative equations affecting AC conductivity. An important properties is that a peak emerges in the mid-IR in the AC conductivity for some α and α_1. It is attributed to the emergence of the pseudo-Goldstone mode, which is the consequence of the competition of SSB and ESB. However, when the ESB dominates over the SSB, the peak disappears.

In the superconducting phase, we first study the properties of the condensation. Since the gauge-axion coupling term $J\mathrm{Tr}[XF^2]$ has no effect on the black hole solution, there are only two theoretical parameter considered in our model (the strength of broken translations α and the gauge coupling parameter a) exerting their influences on the condensation. It is easy to find that with the parameter α increasing, the condensation becomes harder for fixed parameter a, while fixed parameter α with the parameter a increasing, the condensation becomes easier. Such an opposite effect means a competitive relationship between α and a. Similarly, the competitive behavior can be observed in superconducting conductivity.

Then we also study the properties of AC conductivity in the superconducting phase. We respectively explore the effects of coupling parameters (α, a, α_1, α_2) in our model on the conductivity. First, we explore the effect of momentum dissipation on AC conductivity. The features of the conductivity with temperature from normal phase to superconducting phase resemble a two-fluid model as the standard holographic superconductor model [8,9,84], and the holographic Q-lattice superconductor [50], and the holographic superconductor from higher derivative theory [85,86]. Then for the influence of the gauge coupling a, we find that a plays a key role in driving the normal component of the electron fluid forming the superfluid component. Especially, for positive a, it is harder to implement the transition from the normal component of the electron fluid forming the superfluid component. In the end, we explore the effect of the gauge-axion coupling. We find that the coupling parameter α_1 can drive the electron superfluid component forming which is similar with the effect of negative a. The increasing of α_1 leads to a more evident gap in AC conductivity. In addition, we find that the coupling of α_2 plays a completely different role from that of α_1, which is attributed to the effect of condensation field χ.

Acknowledgements We are very grateful to Guoyang Fu, Weijia Li, Peng Liu for helpful discussions and suggestions. This work is supported by the Natural Science Foundation of China under Grant Nos. 11775036, 12147209 and 11975072, Fok Ying Tung Education Foundation under Grant No. 171006, the Liaoning Revitalization Talents Program (Grant No. XLYC1905011), the National 111 Project of China (Grant No. B16009), the Postgraduate Research & Practice Innovation Program of Jiangsu Province (KYCX21_3192), and Top Talent Support Program from Yangzhou University.

Data Availability Statement This manuscript has no associated data or the data will not be deposited. [Authors' comment: This study is purely theoretical, and thus does not yield associated experimental data.]

Funded by SCOAP[3].

References

1. J. Bardeen, L.N. Cooper, J.R. Schrieffer, Microscopic theory of superconductivity. Phys. Rev. **106**, 162 (1957)
2. J. Bardeen, L.N. Cooper, J.R. Schrieffer, Theory of superconductivity. Phys. Rev. **108**, 1175–1204 (1957)
3. H.K. Onnes, The superconductivity of mercury. Commun. Phys. Lab. Univ. Leiden **122**, 122–124 (1911)
4. J.M. Maldacena, The large N limit of superconformal field theories and supergravity. Adv. Theor. Math. Phys. **2**, 231–252 (1998). arXiv:hep-th/9711200
5. S.S. Gubser, I.R. Klebanov, A.M. Polyakov, Gauge theory correlators from noncritical string theory. Phys. Lett. B **428**, 105–114 (1998). arXiv:hep-th/9802109
6. E. Witten, Anti-de Sitter space and holography. Adv. Theor. Math. Phys. **2**, 253–291 (1998). arXiv:hep-th/9802150
7. O. Aharony, S.S. Gubser, J.M. Maldacena, H. Ooguri, Y. Oz, Large N field theories, string theory and gravity. Phys. Rep. **323**, 183–386 (2000). arXiv:hep-th/9905111
8. S.A. Hartnoll, C.P. Herzog, G.T. Horowitz, Building a holographic superconductor. Phys. Rev. Lett. **101**, 031601 (2008). arXiv:0803.3295
9. S.A. Hartnoll, C.P. Herzog, G.T. Horowitz, Holographic superconductors. JHEP **12**, 015 (2008). arXiv:0810.1563
10. G.T. Horowitz, J.E. Santos, D. Tong, Optical conductivity with holographic lattices. JHEP **07**, 168 (2012). arXiv:1204.0519
11. G.T. Horowitz, J.E. Santos, D. Tong, Further evidence for lattice-induced scaling. JHEP **11**, 102 (2012). arXiv:1209.1098
12. Y. Ling, C. Niu, J.-P. Wu, Z.-Y. Xian, H.-B. Zhang, Holographic fermionic liquid with lattices. JHEP **07**, 045 (2013). arXiv:1304.2128
13. Y. Ling, C. Niu, J.-P. Wu, Z.-Y. Xian, Holographic lattice in Einstein-Maxwell-Dilaton gravity. JHEP **11**, 006 (2013). arXiv:1309.4580
14. A. Donos, J.P. Gauntlett, The thermoelectric properties of inhomogeneous holographic lattices. JHEP **01**, 035 (2015). arXiv:1409.6875
15. S.A. Hartnoll, J.E. Santos, Cold planar horizons are floppy. Phys. Rev. D **89**(12), 126002 (2014). arXiv:1403.4612
16. A. Donos, J.P. Gauntlett, Holographic Q-lattices. JHEP **04**, 040 (2014). arXiv:1311.3292
17. A. Donos, J.P. Gauntlett, Novel metals and insulators from holography. JHEP **06**, 007 (2014). arXiv:1401.5077
18. Y. Ling, P. Liu, C. Niu, J.P. Wu, Building a doped Mott system by holography. Phys. Rev. D **92**(8), 086003 (2015). arXiv:1507.02514
19. Y. Ling, P. Liu, J.-P. Wu, A novel insulator by holographic Q-lattices. JHEP **02**, 075 (2016). arXiv:1510.05456
20. A. Donos, S.A. Hartnoll, Interaction-driven localization in holography. Nat. Phys. **9**, 649–655 (2013). arXiv:1212.2998
21. T. Andrade, B. Withers, A simple holographic model of momentum relaxation. JHEP **05**, 101 (2014). arXiv:1311.5157
22. M. Taylor, W. Woodhead, Inhomogeneity simplified. Eur. Phys. J. C **74**(12), 3176 (2014). arXiv:1406.4870
23. K.-Y. Kim, K.K. Kim, Y. Seo, S.-J. Sin, Coherent/incoherent metal transition in a holographic model. JHEP **12**, 170 (2014). arXiv:1409.8346
24. L. Cheng, X.-H. Ge, Z.-Y. Sun, Thermoelectric DC conductivities with momentum dissipation from higher derivative gravity. JHEP **04**, 135 (2015). arXiv:1411.5452
25. X.-H. Ge, Y. Ling, C. Niu, S.-J. Sin, Thermoelectric conductivities, shear viscosity, and stability in an anisotropic linear axion model. Phys. Rev. D **92**(10), 106005 (2015). arXiv:1412.8346
26. T. Andrade, *A simple model of momentum relaxation in Lifshitz holography*. arXiv:1602.00556
27. X.-M. Kuang, E. Papantonopoulos, Building a holographic superconductor with a scalar field coupled kinematically to Einstein tensor. JHEP **08**, 161 (2016). arXiv:1607.04928
28. M.R. Tanhayi, R. Vazirian, Higher-curvature corrections to holographic entanglement with momentum dissipation. Eur. Phys. J. C **78**(2), 162 (2018). arXiv:1610.08080
29. X.M. Kuang, J.P. Wu, Thermal transport and quasi-normal modes in Gauss-Bonnet-axions theory. Phys. Lett. B **770**, 117–123 (2017). arXiv:1702.01490
30. A. Cisterna, M. Hassaine, J. Oliva, M. Rinaldi, Axionic black branes in the k-essence sector of the Horndeski model. Phys. Rev. D **96**(12), 124033 (2017). arXiv:1708.07194
31. A. Cisterna, J. Oliva, Exact black strings and p-branes in general relativity. Class. Quantum Gravity **35**(3), 035012 (2018). arXiv:1708.02916
32. A. Cisterna, C. Erices, X.M. Kuang, M. Rinaldi, Axionic black branes with conformal coupling. Phys. Rev. D **97**(12), 124052 (2018). arXiv:1803.07600
33. M. Baggioli, A. Cisterna, K. Pallikaris, Exploring the black hole spectrum of axionic Horndeski theory. Phys. Rev. D **104**(10), 104067 (2021). arXiv:2106.07458
34. M. Baggioli, B. Goutéraux, E. Kiritsis, W.-J. Li, Higher derivative corrections to incoherent metallic transport in holography. JHEP **03**, 170 (2017). arXiv:1612.05500
35. B. Goutéraux, E. Kiritsis, W.-J. Li, Effective holographic theories of momentum relaxation and violation of conductivity bound. JHEP **04**, 122 (2016). arXiv:1602.01067
36. W.J. Li, J.P. Wu, A simple holographic model for spontaneous breaking of translational symmetry. Eur. Phys. J. C **79**(3), 243 (2019). arXiv:1808.03142
37. K.-B. Huh, H.-S. Jeong, K.-Y. Kim, Y.-W. Sun, Upper bound of the charge diffusion constant in holography. arXiv:2111.07515
38. M. Baggioli, O. Pujolas, On holographic disorder-driven metal-insulator transitions. JHEP **01**, 040 (2017). arXiv:1601.07897
39. M. Ammon, M. Baggioli, A. Jiménez-Alba, A unified description of translational symmetry breaking in holography. JHEP **09**, 124 (2019). arXiv:1904.05785
40. M. Baggioli, Applied holography: a practical mini-course. SpringerBriefs in Physics. Springer (2019)
41. L. Alberte, M. Ammon, A. Jiménez-Alba, M. Baggioli, O. Pujolàs, Holographic phonons. Phys. Rev. Lett. **120**(17), 171602 (2018). arXiv:1711.03100
42. M. Baggioli, W.J. Li, Universal bounds on transport in holographic systems with broken translations. SciPost Phys. **9**(1), 007 (2020). arXiv:2005.06482
43. M. Baggioli, K.Y. Kim, L. Li, W.J. Li, Holographic axion model: a simple gravitational tool for quantum matter. Sci. China Phys. Mech. Astron. **64**(7), 270001 (2021). arXiv:2101.01892
44. Y.-Y. Zhong, W.-J. Li, Transverse Goldstone mode in holographic fluids with broken translations. arXiv:2202.05437
45. D. Vegh, Holography without translational symmetry. arXiv:1301.0537
46. L. Alberte, M. Baggioli, A. Khmelnitsky, O. Pujolas, Solid holography and massive gravity. JHEP **02**, 114 (2016). arXiv:1510.09089
47. X.-M. Kuang, E. Papantonopoulos, G. Siopsis, B. Wang, Building a holographic superconductor with higher-derivative couplings. Phys. Rev. D **88**, 086008 (2013). arXiv:1303.2575
48. J. Alsup, E. Papantonopoulos, G. Siopsis, K. Yeter, Spontaneously generated inhomogeneous phases via holography. Phys. Rev. D **88**(10), 105028 (2013). arXiv:1305.2507
49. G.T. Horowitz, J.E. Santos, General relativity and the cuprates. JHEP **06**, 087 (2013). arXiv:1302.6586
50. Y. Ling, P. Liu, C. Niu, J.-P. Wu, Z.-Y. Xian, Holographic superconductor on Q-lattice. JHEP **02**, 059 (2015). arXiv:1410.6761

51. K.-Y. Kim, K.K. Kim, M. Park, A simple holographic superconductor with momentum relaxation. JHEP **04**, 152 (2015). arXiv:1501.00446
52. T. Andrade, S.A. Gentle, Relaxed superconductors. JHEP **06**, 140 (2015). arXiv:1412.6521
53. H.B. Zeng, J.P. Wu, Holographic superconductors from the massive gravity. Phys. Rev. D **90**(4), 046001 (2014). arXiv:1404.5321
54. J. Erdmenger, B. Herwerth, S. Klug, R. Meyer, K. Schalm, S-wave superconductivity in anisotropic holographic insulators. JHEP **05**, 094 (2015). arXiv:1501.07615
55. M. Baggioli, M. Goykhman, Phases of holographic superconductors with broken translational symmetry. JHEP **07**, 035 (2015). arXiv:1504.05561
56. M. Baggioli, M. Goykhman, Under the dome: doped holographic superconductors with broken translational symmetry. JHEP **01**, 011 (2016). arXiv:1510.06363
57. Y. Ling, P. Liu, J.P. Wu, W.H. Wu, Holographic superconductor on a novel insulator. Chin. Phys. C **42**(1), 013106 (2018). arXiv:1711.07720
58. H.-S. Jeong, K.-Y. Kim, Homes' law in holographic superconductor with linear-T resistivity. arXiv:2112.01153
59. S.S. Gubser, F.D. Rocha, Peculiar properties of a charged dilatonic black hole in AdS_5. Phys. Rev. D **81**, 046001 (2010). arXiv:0911.2898
60. Y.-S. An, T. Ji, L. Li, Magnetotransport and complexity of holographic metal-insulator transitions. JHEP **10**, 023 (2020). arXiv:2007.13918
61. X.-J. Wang, W.-J. Li, Holographic phonons by gauge-axion coupling. JHEP **07**, 131 (2021). arXiv:2105.07225
62. N. Iqbal, H. Liu, Universality of the hydrodynamic limit in AdS/CFT and the membrane paradigm. Phys. Rev. D **79**, 025023 (2009). arXiv:0809.3808
63. A. Donos, J.P. Gauntlett, Thermoelectric DC conductivities from black hole horizons. JHEP **11**, 081 (2014). arXiv:1406.4742
64. A. Amoretti, A. Braggio, N. Maggiore, N. Magnoli, D. Musso, Analytic dc thermoelectric conductivities in holography with massive gravitons. Phys. Rev. D **91**(2), 025002 (2015). arXiv:1407.0306
65. A. Donos, J.P. Gauntlett, Navier–Stokes equations on black hole horizons and DC thermoelectric conductivity. Phys. Rev. D **92**(12), 121901 (2015). arXiv:1506.01360
66. Y. Ling, P. Liu, J.P. Wu, Z. Zhou, Holographic metal-insulator transition in higher derivative gravity. Phys. Lett. B **766**, 41–48 (2017). arXiv:1606.07866
67. M. Baggioli, Gravity, holography and applications to condensed matter. PhD thesis, Barcelona, Autonoma U. (2016). arXiv:1610.02681
68. Y. Ling, Holographic lattices and metal-insulator transition. Int. J. Mod. Phys. A **30**(28), 1545013 (2015)
69. Y. Ling, P. Liu, C. Niu, J.-P. Wu, Z.-Y. Xian, Holographic entanglement entropy close to quantum phase transitions. JHEP **04**, 114 (2016). arXiv:1502.03661
70. Y. Ling, P. Liu, J.P. Wu, Characterization of quantum phase transition using holographic entanglement entropy. Phys. Rev. D **93**(12), 126004 (2016). arXiv:1604.04857
71. M. Baggioli, O. Pujolas, Electron-phonon interactions, metal-insulator transitions, and holographic massive gravity. Phys. Rev. Lett. **114**(25), 251602 (2015). arXiv:1411.1003
72. M. Baggioli, O. Pujolas, On effective holographic Mott insulators. JHEP **12**, 107 (2016). arXiv:1604.08915
73. A. Donos, B. Goutéraux, E. Kiritsis, Holographic metals and insulators with helical symmetry. JHEP **09**, 038 (2014). arXiv:1406.6351
74. E. Kiritsis, J. Ren, On holographic insulators and supersolids. JHEP **09**, 168 (2015). arXiv:1503.03481
75. S.A. Hartnoll, P.K. Kovtun, M. Muller, S. Sachdev, Theory of the Nernst effect near quantum phase transitions in condensed matter, and in dyonic black holes. Phys. Rev. B **76**, 144502 (2007). arXiv:0706.3215
76. S.A. Hartnoll, D.M. Hofman, Locally critical resistivities from Umklapp scattering. Phys. Rev. Lett. **108**, 241601 (2012). arXiv:1201.3917
77. A. Lucas, S. Sachdev, Memory matrix theory of magneto transport in strange metals. Phys. Rev. B **91**(19), 195122 (2015). arXiv:1502.04704
78. R. Mahajan, M. Barkeshli, S.A. Hartnoll, Non-Fermi liquids and the Wiedemann-Franz law. Phys. Rev. B **88**, 125107 (2013). arXiv:1304.4249
79. J.P. Wu, X.M. Kuang, Z. Zhou, Holographic transports from Born-Infeld electrodynamics with momentum dissipation. Eur. Phys. J. C **78**(11), 900 (2018). arXiv:1805.07904
80. R.A. Davison, B. Goutéraux, Dissecting holographic conductivities. JHEP **09**, 090 (2015). arXiv:1505.05092
81. Z. Zhou, Y. Ling, J.P. Wu, Holographic incoherent transport in Einstein-Maxwell-dilaton gravity. Phys. Rev. D **94**(10), 106015 (2016). arXiv:1512.01434
82. E. Kiritsis, L. Li, Holographic competition of phases and superconductivity. JHEP **01**, 147 (2016). arXiv:1510.00020
83. W. Cai, S.J. Sin, The superconducting dome for holographic doped Mott insulator with hyperscaling violation. Eur. Phys. J. C **81**(6), 565 (2021). arXiv:2009.00381
84. G.T. Horowitz, Introduction to holographic superconductors. Lect. Notes Phys. **828**, 313–347 (2011). arXiv:1002.1722
85. J.P. Wu, P. Liu, Holographic superconductivity from higher derivative theory. Phys. Lett. B **774**, 527–532 (2017). arXiv:1710.07971
86. Y. Liu, G. Fu, H.-L. Li, J.-P. Wu, X. Zhang, Holographic p-wave superconductivity from higher derivative theory. Eur. Phys. J. C **81**, 568 (2021). arXiv:2011.07330